

Experimental Determination of Material Properties for Inflatable Aeroshell Structures



AE8900 MS Special Problems Report
Space Systems Design Lab (SSDL)
Guggenheim School of Aerospace Engineering
Georgia Institute of Technology
Atlanta, GA

Author:
Allison L. Hutchings

Advisor:
Dr. Robert D. Braun

May 26, 2009

Experimental Determination of Material Properties for Inflatable Aeroshell Structures

Allison L. Hutchings
Georgia Institute of Technology, Atlanta, GA, 30332

Dr. Robert Braun
Advisor, Georgia Institute of Technology, Atlanta, GA, 30332

As part of a deployable aeroshell development effort, system design, materials evaluation, and analysis methods are under investigation. One specific objective is to validate finite element analysis techniques used to predict the deformation and stress fields of aeroshell inflatable structures under aerodynamic loads. In this paper, we discuss the results of an experimental mechanics study conducted to ensure that the material inputs to the finite element models accurately predict the load elongation characteristics of the coated woven fabric materials used in deployable aeroshells. These coated woven fabrics exhibit some unique behaviors under load that make the establishment of a common set of test protocols difficult. The stiffness of a woven fabric material will be influenced by its biaxial load state. Uniaxial strip tensile testing although quick and informative may not accurately capture the needed structural model inputs. Woven fabrics, when loaded in the bias direction relative to the warp and fill axes, have a resultant stiffness that is quite low as compared with the warp and fill directional stiffness. We evaluate the experimental results from two load versus elongation test devices. Test method recommendations are made based on the relevance and accuracy of these devices. Experimental work is conducted on a sample set of materials, consisting of four fabrics of varying stiffness and strength. The building blocks of a mechanical property database for future aeroshell design efforts are constructed.

Nomenclature

E	= Young's modulus	ε	= strain
G	= shear modulus	γ	= shear strain
J	= polar moment of inertia	ϕ	= rotation angle
T	= torque	σ	= stress
p	= internal pressure	τ	= shear stress
r	= radius	ν	= Poisson's ratio
t	= thickness		
Δx	= length of rotation		

Subscripts

h	= hoop direction
l	= longitudinal direction
1	= 1 st principal direction
2	= 2 nd principal direction

Acronyms

IAD	= Inflatable Aerodynamic Decelerator
IRVE	= Inflatable ReEntry Vehicle Experiment
PAIDAE	= Program to Advance Inflatable Decelerators for Atmospheric Entry

I. Introduction

ALL previous missions to land on Mars have used supersonic parachutes for deceleration after descending through the hypersonic regime. Due to the desire to land higher mass systems, better technologies for supersonic and new technologies for hypersonic deceleration may be necessary. Inflatable Aerodynamic Decelerators (IADs) are a technology currently being researched for use on high mass missions with application to Martian entry. Accurate modeling is required of the deformation and stress fields of aeroshell inflatable structures under aerodynamic loads during descent. Because these finite element analysis results will only be as accurate as the inputs, one area in need of advancement is the determination of the mechanical properties of these materials. The goal of the current study is to investigate experimental methods for this process and determine if assumptions about the linear elastic behavior of the materials is valid. The general characteristics of woven fabric are presented and a review of previous test methods is compared. The test methodology chosen and samples of corresponding results from both uniaxial and biaxial testing are shown.

This paper provides a review of the different mechanical tests conducted at the Georgia Institute of Technology in spring 2009. It briefly discusses the importance of material characterization to Entry, Descent, and Landing research for simulation of IADs.

II. The Importance of Material Characterization to Entry, Descent, and Landing

All missions to reach Mars since the Viking lander have scaled the successful deceleration technology of supersonic parachutes. Future missions with heavier payloads will reach the limit of this technology due the deployment restrictions on these parachutes for large masses [1]. Preliminary research shows that an IAD can be deployed at a higher Mach number and higher dynamic pressure than a corresponding supersonic parachute, thus allowing a longer timeline for higher altitude and higher mass landings [2]. Multiple relevant IAD shapes are being investigated, including the tension shell, the isotenoid and the Inflatable ReEntry Vehicle Experiment (IRVE), seen in Figure 1. IRVE is a test flight of a stacked toroid inflatable decelerator concept. Like a parachute, an IAD must be made of a high strength but flexible material so it can be packaged into a small volume for flight. Due to the nature of coated woven fabrics, these inflatable structures will have complex deformations and both the stress fields from the fluid-structure interaction during reentry and the mechanics of these materials must be understood.

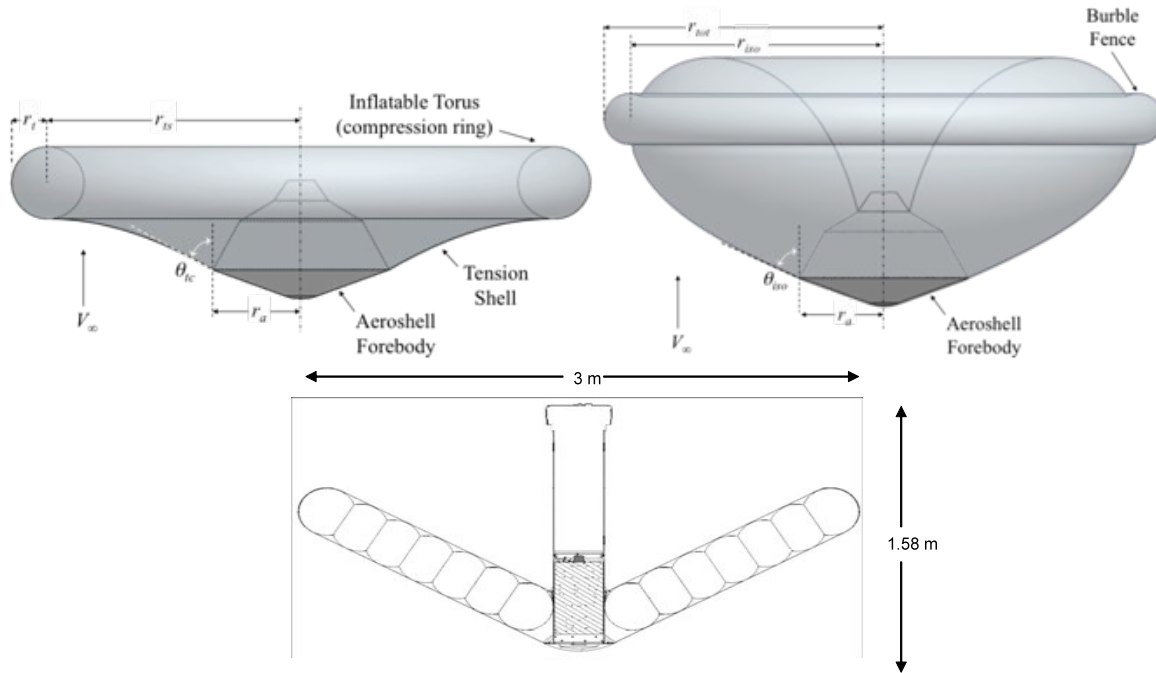


Figure 1. Example of three IAD shapes: the tension shell, the isotenoid and IRVE. [2], [3].

III. Background

A. Coated Woven Fabrics

Coated woven fabrics exhibit unique behaviors while under loading, including a stiffness which can be strongly influenced by the load state. For inflatable structures the load is biaxial, so uniaxial strip tensile testing may not accurately capture all the inputs necessary for a structural model. Fabrics are woven with two primary axes, the warp and the fill, which can have differing mechanical properties. An illustration of these primary axes is shown in Figure 2. Two characteristics that influence these differences are the yarns per inch along each axis and the degree of crimp interchange between the warp and fill yarn systems. Two distinct phases in the extensibility of woven fabrics are crimp removal and yarn elongation. Under uniaxial loading, crimp removal will occur early in the load versus elongation response and has a low relative stiffness. An illustration of the crimp in a yarn is shown in Figure 2. Yarn elongation occurs later in the load versus elongation response and has a high relative stiffness driven by the elastic modulus of the yarn itself. Woven fabrics, when loaded in the bias direction, have a resultant stiffness that is quite low as compared with the warp and fill directions. The bias stiffness is most easily visualized with the picture frame shear test shown on the right in Figure 2. For woven fabrics there exists a shear locking angle. When the shear locking angle is reached the threads are physically jammed up, and with no in plane preload, buckling occurs.

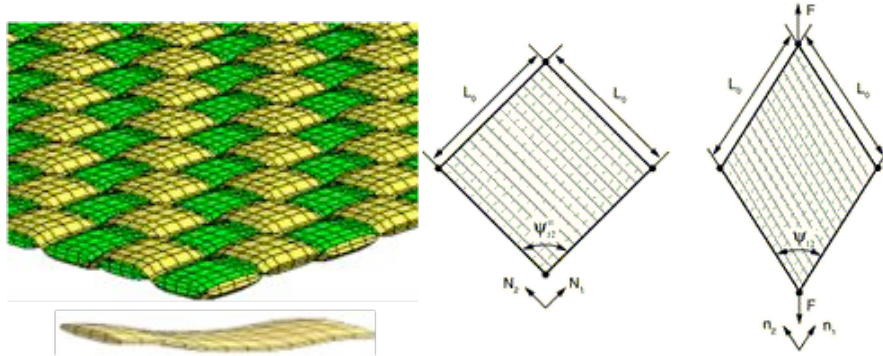


Figure 2. Left: Example of a plain weave fabric and the principal directions and a single crimped yarn [4]
Right: Picture frame shear test [5].

B. Linear Elastic Hooke's Law for Lamina

One of the first decisions that influence the necessary experimental mechanics is the level of refinement chosen in modeling the fabric itself. The finite element modeling of woven fabric inflatable structures typically includes some degree of homogenization of the actual material construction. Even for cases, such as woven fabric ballistic impact barriers, where the actual yarns are modeled as solid elements, homogenization is required to transform a continuous strand of twisted fibers into a uniform solid yarn. Our objective is to conduct sufficient experimental work so that we can directly achieve a homogenization where the coated fabric construction is modeled as a through the thickness homogeneous membrane or shell. Given the level of approximation we have defined for the fabric construction, we can discuss the material law to be used for this formulation. Depending on the methodology chosen the level of fidelity and complexity vary greatly. A select few are presented here to support the discussion:

- Linear elastic orthotropic
- Hybrid constructions
- Hyperelastic orthotropic
- User defined material law specifically developed for woven fabrics

Linear elastic materials are the most straightforward and easy to implement of these options. Hybrid constructions involve the overlaying or smearing of different element formulations on top of each other. By assigning specific material stiffness to the individual components, the construction can be tuned to match test results. The hybrid method can be rather time consuming and may not necessarily result in a direct or unique answer. Both hyperelastic orthotropic and user defined material laws would involve some level of detailed theoretical derivation and programming to implement. Prior to making this type of investment in time and effort, our goal is to determine if the linear elastic Hooke's law provides sufficient accuracy to meet the needs of IAD development teams.

For shell and membrane formulations the plane stress representation is implemented. The compliance matrix and stress-strain equations for a linear elastic orthotropic material becomes.

$$\begin{Bmatrix} \varepsilon_1 \\ \varepsilon_2 \\ \gamma_{12} \end{Bmatrix} = \begin{bmatrix} 1/E_1 & -\nu_{12}/E_1 & 0 \\ -\nu_{21}/E_2 & 1/E_2 & 0 \\ 0 & 0 & 1/G_{12} \end{bmatrix} \begin{Bmatrix} \sigma_1 \\ \sigma_2 \\ \tau_{12} \end{Bmatrix} \quad (1)$$

From orthotropic reciprocity we also have that $\nu_{12}/E_1 = \nu_{21}/E_2$, which results in four equations and five unknowns. In order to avoid negative strain energy, material stability requires that E_1, E_2, G_{12} and $|\nu_{12}| < (E_1/E_2)^{1/2}$. The experimental need is thus to conduct testing to eliminate some of the unknowns and if necessary solve for any remaining unknowns not captured directly in test while ensuring that stability is met.

IV. Literature Review

Two previous studies completed extensive literature reviews of bi-axial fabric-material test techniques. The first by Bassett, Postle, and Pan provides a history of biaxial testing for apparel type fabrics [6]. Though the materials to be tested in this study are structural fabrics, the test methods are still relevant. In the second, Reinhart gives a review of the three main types of biaxial testing with applications for lightweight structural fabric for large scale tent structures [7]. These tests have common issues with the non-linearity of fabric behavior due to interactions between the woven yarns. Unlike traditional composites there is no hardened matrix to prevent relative motion between the weave. Due to this motion, the mechanical properties (moduli in warp and fill and shear modulus) are interconnected. Also, the current stress and strain is time dependent on prior loading of the material. In most biaxial testing literature, this effect is ignored and the material is assumed to be “ideally elastic” [6].

A. Uniaxial Testing

The methodology behind uniaxial testing for fabrics is standardized by ASTM D-5035-06, “Standard Test Method for Breaking Force and Elongation of Textile Fabrics (Strip Method)” [8]. This test is done with type 1R specimens, which are 1.0 inch wide raveled strips. The test is performed using a constant rate of extension at a rate of 12 inches per minute. Typically elongation, which is used to compute strain, is tracked with an optical method or an extensometer.

B. Planar Testing

The most commonly accepted method for biaxial tensile testing is a planar tension test with force applied independently in two axes to a square of fabric. Many different test devices of this type have been built [6], [7]. The applied load causes an approximate uniaxial stress in the “arms” of the specimen near the clamps and a biaxial state at the center. Complexities arise in the method of gripping the fabric, which include pin clamps, “grab” clamps, and cruciform clamps [6]. Each of these methods introduces force to the specimen differently. Stress measurement is another area of concern because it is assumed to be force per unit length along the clamps, which depending on the clamping method can induce error. Strain is measured close to the center of the sample via an optical measurement or with an extensometer.

A variation of this type of test apparatus can be made to interface with a generic compression testing machine by creating a “four bar linkage” assembly around the specimen [9]. When the compression is applied, the linkages cause the sample to experience extension. If the testing machine has the capability for torsion, shear can also be tested with the same setup. The advantage to this technique is that there is no need for a separate method to apply force (such as numerous actuators). The disadvantage is that the linkage system only allows equibiaxial extension.

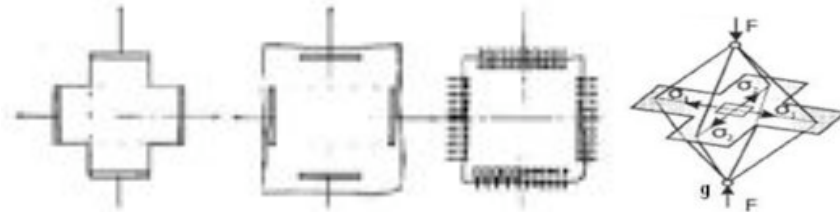


Figure 3. Example planar test grip methods and a four-bar linkage diagram [10].

Planar testing is often used to determine the shear behavior of fabrics. The primary method is with a test setup that measures the resistance of the fabric to relative motion of two clamps. To prevent immediate buckling of the specimen, a uniaxial tensile stress must also be applied. The test results are extremely dependent on whether the clamps stay parallel and the ratio of clamp width to sample length. A higher ratio lessens the dependence on the applied uniaxial load [6]. A second commonly used method is a uniaxial test of a biased fabric sample (commonly 45 degrees). This approach had been used successfully with hardened composites to measure shear, but is strongly discouraged for fabric testing as the extreme contraction at the center of the specimen in combination with the inability for contraction at the clamped ends can cause an overestimation of shear measurements by 20 to 300 percent.

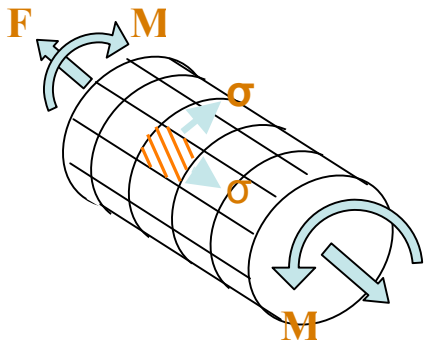


Figure 4. Example of cylindrical test stresses and forces.

The major disadvantage to this test is that it requires a seam to create the cylindrical shape. Also, if the fabric has any permeability, the ratio of stresses cannot be controlled precisely.

One interesting test using this method was completed by Said at Goddard Space Flight Center [11], which used cylindrical testing to measure Young's moduli in both the warp and fill directions along with both Poisson ratios. The stress was solved for from the classical equations for a cylindrical pressure vessel. A detailed example of a vertically implemented cylinder tension/torsion test is provided in [12]. This paper points out that cylinder testing is important for structural fabrics because stiffness, which is dependent on the internal pressure, is generally more important than the strength in inflatable applications.

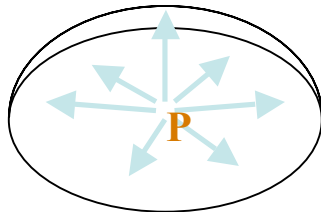


Figure 5. Disk test layout.

C. Cylindrical Testing

The cylindrical test involves using internal pressure to cause a two-to-one circumferential versus axial stress ratio. Additional tension and/or torsion can be applied to change the axial and shear stresses. This method, like the planar tensile test, is commonly used and the stress

D. Disk Testing

A final method, not often used, is the burst or disk test where a circular specimen is clamped and a pressure is applied via air or a fluid [9]. The deflection as a function of pressure is measured and using assumptions of spherical behavior, burst strength can be determined. Disadvantages of this approach include the fact that the ratio of stresses cannot be varied, and since the behavior of the material is anisotropic, the assumptions of spherical behavior are incorrect. The main advantage of this method is that the test is simpler to conduct than either the cylindrical or planar methods.

V. Test Setup

Material testing was performed to obtain experimental data sets for four candidate fabric materials. By testing a collection of potential aeroshell materials this investigation is able to evaluate the suitability of each proposed test method, and provide mechanical property data for consideration in aeroshell preliminary design trade studies. This data was collected through three different test setups: a uniaxial tension test, a biaxial cylinder inflation test (with or without torsion) and a biaxial disk test. In each test, the general methodology is the same. A load is applied through tension, inflation, torsion, or some combination of these three, and the load versus deformation is recorded for increasing increments of load. The deformation in the specimens is used to determine the strain at each load point. Stress is estimated using the known load and the load measured shape of the specimen. The stress-strain information is used to determine the mechanical properties.

A. Candidate Materials

In this investigation, four candidate fabric materials (presented in Table 1) were studied: two silicone coated Kevlar layups used in previous projects, a Vectran used on the MER/MPF airbag bladders, and a Kapton coated Kevlar that ILC is investigating. The first of the Kevlar materials was used for the Inflatable Re-Entry Vehicle Experiment, or IRVE, a test flight of a stacked toroid inflatable decelerator concept. The second was for wind tunnel testing of tension cone models at the NASA Glenn supersonic tunnel for the Program to Advance Inflatable Decelerators for Atmospheric Entry, or PAIDAE. The Kapton coated Kevlar is presently under examination for use in construction of double-walled structures.

Table 1. The materials list for the study.

Material	Lay Up	Thickness (mils)
PAIDAE	Double sided urethane coated Kevlar	10
IRVE	Calendared, single sided silicone coated Kevlar	7.87
MER/MPF	Single sided silicone coated Vectran	7.5
ILC Mat.	Kapton coated Kevlar	6

B. Uniaxial Testing

Except for a few deviations, the uniaxial testing is done in accordance with ASTM D-5035-06, as described in Section IV. The test specimens are one by six inch samples. One difference with the standard is the speed of the test was set to 2 inches per minute instead of the standard 12 inches per minute in order to match a baseline value established in ILC Dover testing. As part of the design process, strain rate sensitivity would be confirmed once the materials trade space is narrowed. Also, the face of the grip is textured instead of the ideal smooth finish. This deviation is mitigated with use of card stock between the sample and the jaw.

Each sample is mounted securely in the clamp, like shown in Figure 6 above, taking care that the long dimension is as parallel as possible to the direction of the applied force. Though not ideal, elongation is measured simply with the grip displacement due to lack of other measurement methods currently available. Based on the specimen markings at each jaw, no noticeable slippage was observed.



Figure 6. Sample held in the grips with card stock to prevent jaw breakage.

C. Cylindrical Biaxial Testing

The sample holder for the cylinder tests is used for both inflation and torsion testing. A 7.5-inch diameter cylinder is mounted to rigid plates at each end as shown in Figure 7. The test conditions performed for the cylinder testing are shown below in Table 2. Each inflation test tracks the deformation at 10 states of increasing pressure up to a predefined maximum. The torsion test tracks the deformation at states in increments of 2.5 degrees up to a maximum maintainable torque. Each state consists of the torque needed to reach the specified angle of rotation (Φ).

Table 2. Cylinder tests.

Material	Direction	# of Tests	Sub-Tests
PAIDAE	Warp	3	Inflation & Torsion
	Fill	3	Inflation & Torsion
IRVE	Warp	3	Inflation & Torsion
	Fill	3	Inflation & Torsion
MER/MPF	Warp	3	Inflation & Torsion
	Fill	3	Inflation & Torsion
ILC Mat.	Warp	3	Inflation & Torsion
	Fill	3	Inflation & Torsion

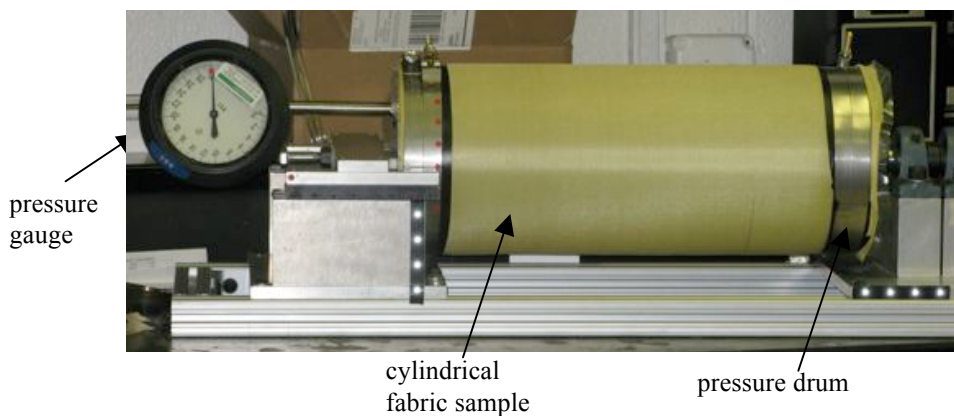


Figure 7. The cylinder torsion device.

D. Disk Biaxial Testing

The sample holder for the disk test consists of a simple plate and top ring, shown in Figure 8. This setup allows a 12-inch diameter circular hole for the fabric disk to deflect. The system is held together with 8 ½-inch bolts from above. A pressure port is tapped in the center of the plate to apply uniform loading to the sample's underside, which is accessed with a channel for the inflation line on the bottom of the plate. This setup is clamped to a table via the bottom plate only so that the samples can be removed without re-clamping. The system is sealed against leakage via an O-ring located on the top face of the bottom plate. The disk tests performed are listed in Table 3 below.

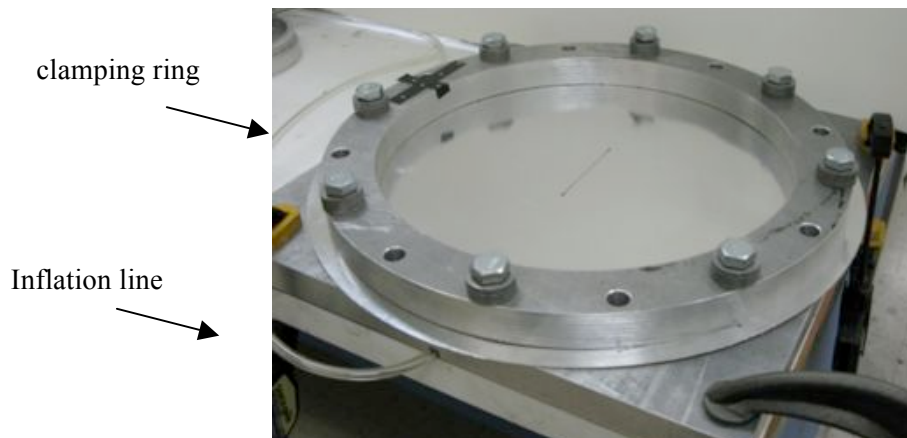


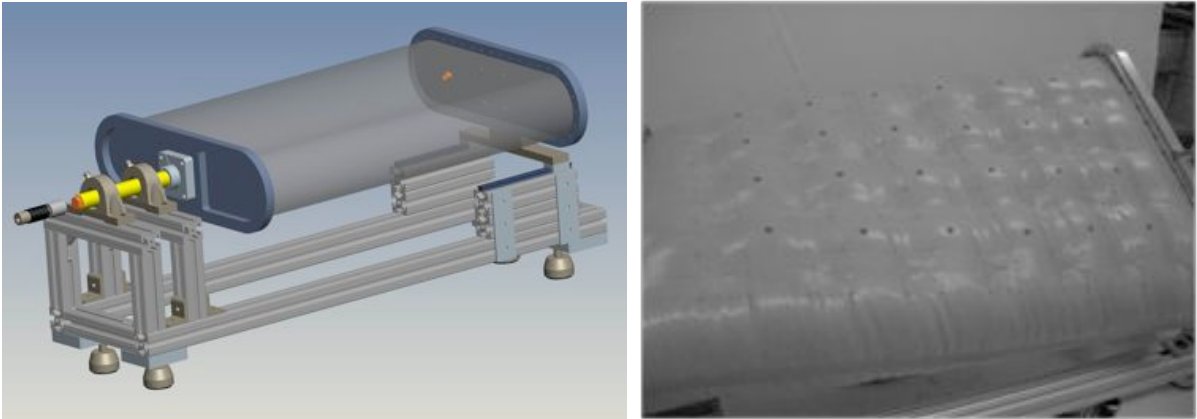
Figure 8. The disk test device with a sample of the ILC Material.

Table 3. Disk tests.

Material	# of Tests	Tests
PAIDAE	3	Inflation
IRVE	3	Inflation
MER/MPF	3	Inflation
ILC Mat.	3	Inflation

E. Element Testing

The final piece of testing was load versus elongation on two different “element” shapes to test different construction methods for eventual comparison to finite element modeling. The uniaxial, cylinder, and disk tests were conducted to help establish material properties. Element testing is being conducted to both evaluate proposed aeroshell construction components, but to also to provide experimental data where the accuracy of finite element predictions can be validated. The two shapes are the dual wall planar shape (seen in Figure 9) and a larger cylinder and each has two test articles, one out of the PAIDAE material and one out of the ILC Material. The dual wall panel would be used as a structural element to evolve the conical shape of an IAD. Inflated cylindrical tubes would be used for underlying support of the dual wall panel or as a compression ring. Each article was tested both in torsion to 45 degrees with inflation pressures up to 10 psi. The test matrix for the elements is provided in Table 4.

**Figure 9. Dual-wall test article with example of a torsion state.****Table 4. Element tests.**

Material	Shape	# of Tests	Sub-Tests
PAIDAE	Cylinder	1	Torsion
ILC Mat.	Cylinder	1	Torsion
PAIDAE	Dual-Wall	1	Torsion
ILC Mat.	Dual-Wall	1	Torsion

VI. Analysis Procedure

A. Photogrammetry

Photogrammetry is a measurement technique used to estimate the 3-dimensional coordinates of points on an object. A simple photogrammetry system was set up with a high-end point-and-shoot digital camera with a manual mode (Canon Powershot G9) on a tripod. Four photographs were taken at each state of the test. Details of the test set up followed that done in [13] and [14]. Examples of the photos and the estimated coordinates from those photos for the cylinder and disk shapes are seen in Figure 10. Post processing of the photogrammetry data provides the trajectory of a discrete set of material points as load is applied. This discrete set of material points corresponds to the locations where the targets were attached to the inflatable structure. With the kinematics known at these discrete points, the calculation of the displacement vector is possible. When the photogrammetry targets are laid out in a grid type manner as in Figure 10, the spatial derivatives of the displacement vector can be easily approximated. The

displacement vector data also can be interpolated to finer resolution grids to result in more accurate derivative approximations. In either case, the Lagrangian strain tensor is computed with the displacement vector spatial derivatives.

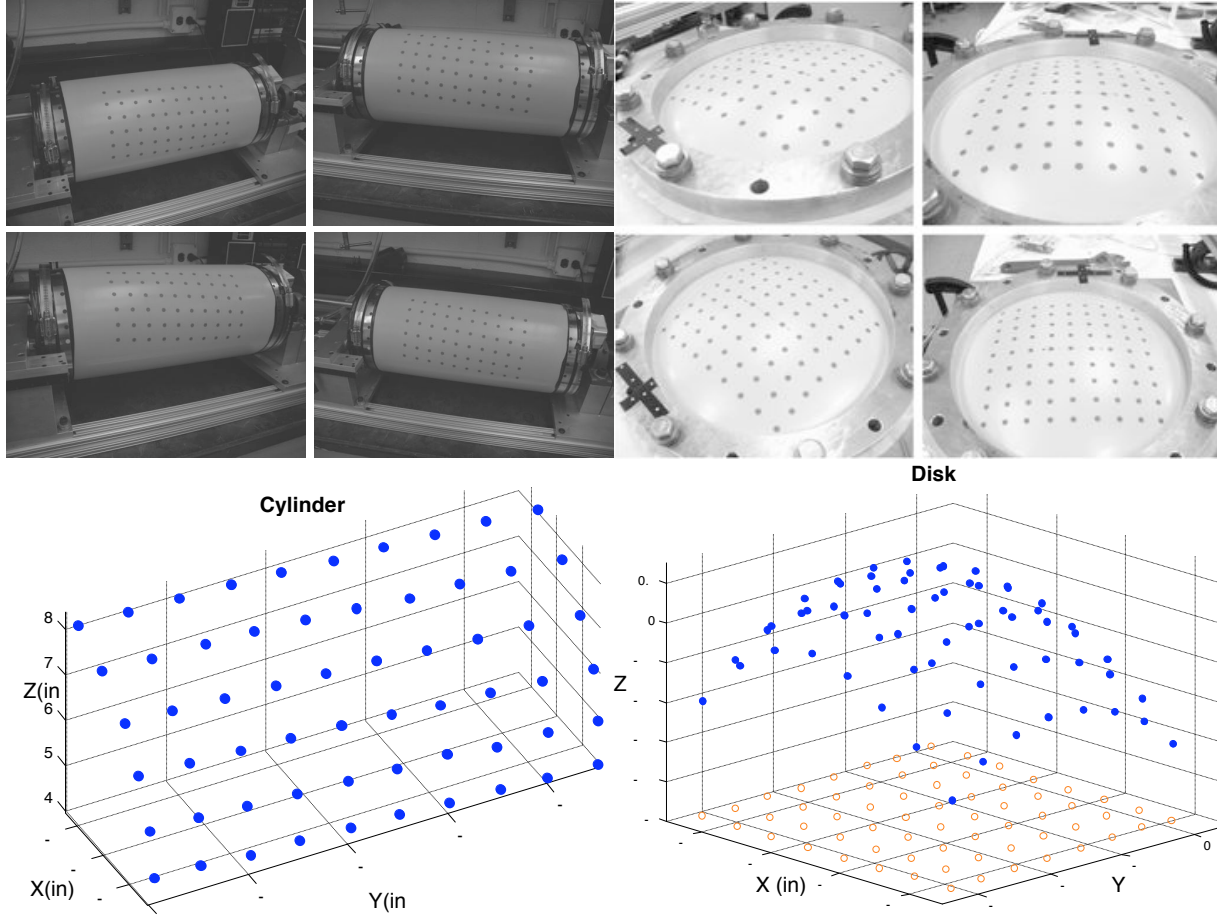


Figure 10. Example set of data for one state of photogrammetry for a cylinder and a disk. Left: The four photos required to determine the 3-dimensional positions of the points on the cylinder and the determined points from the surface for this state of torsion. Right: The four photos required to determine the 3-dimensional positions of the points on the disk and the determined points from the surface for this state of inflation.

B. Material Properties Determination

Young's Modulus from uniaxial testing was found via the slope of the linear portion of the stress strain curve (the linear elastic model for the orthotropic material was presented in Section III). In addition to defining the response to uniaxial load, the same test may be used to generate an initial estimate of stiffness range under biaxial load. As noted in Section III, the uniaxial response may be bilinear. In these cases the slopes of these two distinct linear regions will bound the expected biaxial modulus so that an initial estimate is made as the average of these two slope values.

The shear modulus is estimated from the cylinder test. Based on the stress state of a pressure vessel, the load in the cylinder is defined as $\sigma_h = pr/t$ and $\sigma_l = pr/2t$ in the hoop and longitudinal directions, where the hoop and longitudinal stresses correspond to the two principal stresses in the material. These correlate to either the warp or fill directions of the fabric depending on the orientation of the specimen. Using the measured strains from photogrammetry and the calculated stress from the inflation pressure, the mechanical properties can be found.

The shear modulus (G) can be determined from the cylinder torsion test. The parallel end plates from the cylinder test allow both an assumption of behavior as a thin walled cylindrical tube and linear Hookean material properties. As such, the shear stress (τ) can be assumed uniformly distributed over the cross-section with $\tau = G\gamma$. The shear strains (γ) are computed using shaft length (Δx), the radius of the cylinder (r), and the angle through which it has been twisted (ϕ). The value γ is defined for small values as, $\gamma = r\Delta\phi / \Delta x$. This relation is shown visually in Figure 11. The shear stress can be determined from $\tau = Tr/J$ where J is the polar moment of inertia, which can be defined as $J = \pi r^3 t$ for a thin walled cylinder.

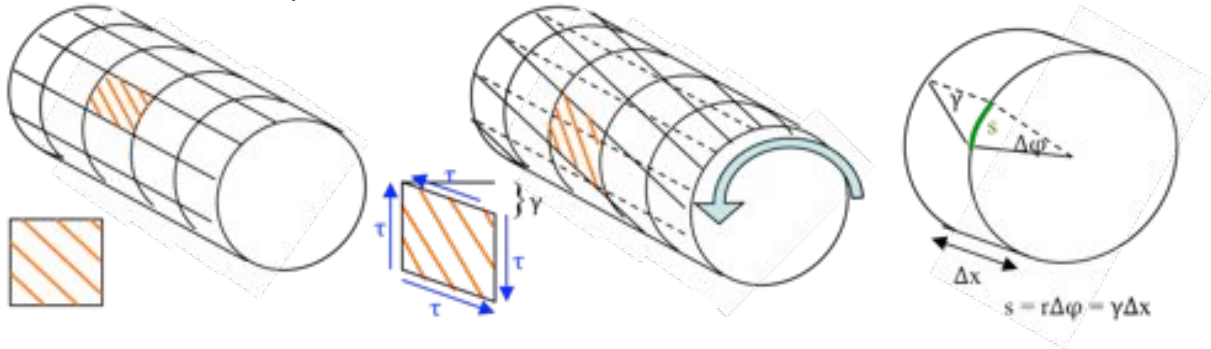


Figure 11. The shearing strains induced from the applied angular motion.

The disk test setup also uses orthotropic specimens, but unlike the cylinders which strain in the principal directions, the disk deflects as a function of the two different sets of fibers. An isotropic disk would deflect into the shape of a spherical cap, but the orthotropic disk forms an ellipsoidal cap. The stresses along the two major axes in the disk can be approximated as those from two spheres of different radii, where once again the stress is $\sigma = pr/2t$.

VII. Test Results

A. Uniaxial Testing

The uniaxial results are presented in Table 5, and with the resulting plots in Figures 20-23 in Appendix A. The uniaxial modulus is taken as the slope of the final linear region of the stress strain curve. The estimated biaxial modulus is the average of the two bilinear regions. For both modulus values the error is conservatively estimated from the standard deviation from the mean instead of propagated because this results in a higher spread.

Table 5. Stiffness Results for the different materials from uniaxial testing.

Material	Direction		Uniaxial (ksi)	Estimated Biaxial (ksi)
PAIDAE	Warp	E_1	1940±70	1200±80
	Fill	E_2	1930±100	1190±70
IRVE	Warp	E_1	1350±60	1030±160
	Fill	E_2	1220±40	690±10
ILC Mat.	Warp	E_1	2060±200	1560±260
	Fill	E_2	1410±200 ¹	940±260
MER/MPF	Warp	E_1	1940±90	1340±60
	Fill	E_2	1130±140	590±70

¹ There were not enough successful samples in the fill direction of the Kapton coated Kevlar being investigated by ILC to get a standard deviation from the mean value, instead the mean from the warp direction was used.

B. Biaxial Testing

Results for the cylinder biaxial testing are shown in Figures 24-27 in Appendix B. The tests were completed to angles of up to 30 degrees for the silicone coated Kevlar and the Vectran, up to 20 degrees for the urethane coated Kevlar, and up to 5 degrees for the Kapton coated Kevlar. This produced torque values of up to 38 ft-lb for the urethane coated Kevlar cases. The current estimates of shear modulus are presented in Table 6. These estimates are for the shear of the cylinder as the fibers in the warp or fill direction are aligned with the test setup.

Table 6. Results from the cylinder shear modulus testing.

Material	Direction	G (ksi)
PAIDAE	Warp	5.30±0.15
	Fill	4.75±0.15
IRVE	Warp	2.40±0.50
	Fill	2.50±0.40
ILC Mat.	Warp	25.4±0.85
	Fill	21.7±0.85
MER/MPF	Warp	2.86±0.30
	Fill	2.16±0.20

Results from the disk tests are presented in Figures 28-29 in Appendix C. The tests were run from 0 to 10 psi for each of the samples. The warp result for the Vectran material shows a trend seen in some woven fabric systems of a knee where the data bends over after some initial strain [11]. Both the IRVE material and the MER/MPF material showed nonlinear behavior and the IRVE material was not monotonic. Due to this an apparent modulus was not estimated for these two materials. An apparent stiffness was calculated for the PAIDAE and ILC materials by assuming a low dependence on Poisson's ratio. The results are shown in Table 7. Note that these slopes are not the orthotropic moduli because of the low dependence on the Poisson's ratio. These properties must be calculated using an advanced material model, or with a more comprehensive biaxial test setup as discussed in IX.

Table 7. Results from the disk testing

Material	Direction	Apparent Moduli (ksi)
PAIDAE	Warp	1840±320
	Fill	1760±380
ILC Mat.	Warp	2130±170
	Fill	1780±70

C. Element Testing

The element testing data is important both to demonstrate the feasibility of new construction techniques and for use in correlating determined mechanical properties with analysis results from finite element modeling. The torsion result for the IRVE dual-wall element is shown in Figure 12. In this case, the stiffness of the element increases with internal pressure causing the slope of the line to change. The Kevlar is flexible and did not buckle even at the highest angles of torsion.

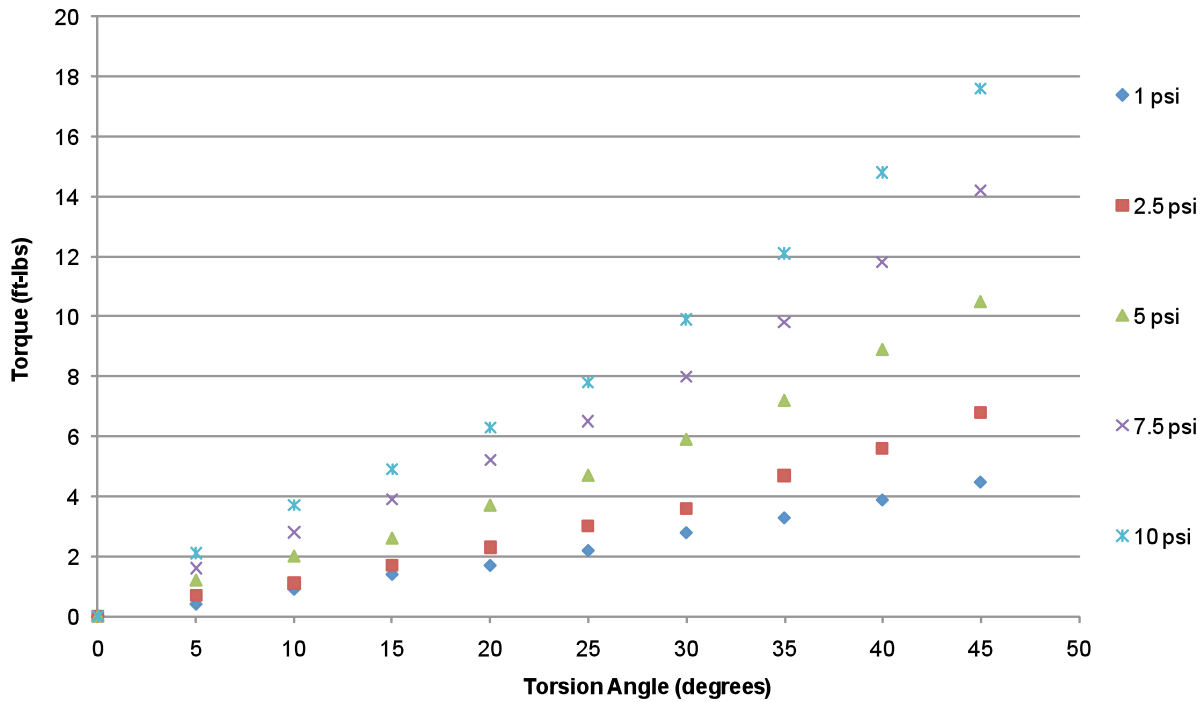


Figure 12. Single sided silicone coated Kevlar dual-wall cylinder torsion results for increasing inflation pressures. The trends show a linear relationship between torque and angle for the varying inflation pressures.

The torsion results for the Kapton coated Kevlar are shown in Figure 13. This ILC material had much higher stiffness than the IRVE material, but it began to wrinkle at around 10 degrees. At each inflation pressure the test was run to a maximum angle at which the torque values began to level off or drop. For the lower pressures this occurred at 10 degrees and it increases to 30 or 35 degrees maximum. It is important to note that the element was in a state of wrinkling before these points, but the torque required was still increasing.

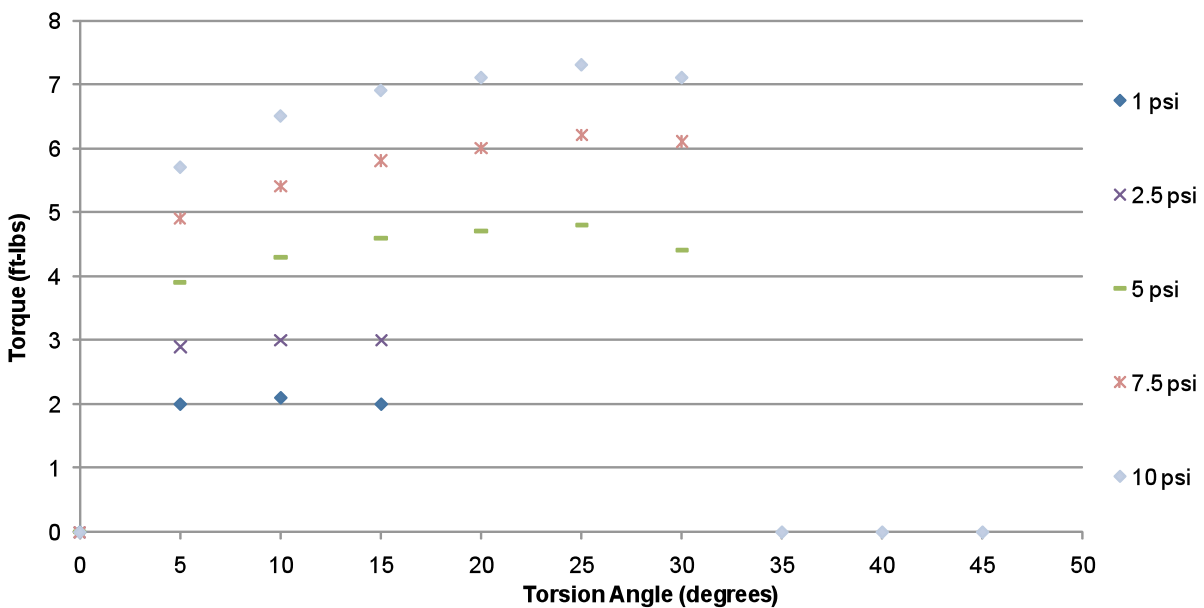


Figure 13. Kapton coated Kevlar dual-wall torsion results for increasing inflation pressures.

The torsion results for the two cylinders exhibited similar trends. The results for the IRVE material are seen in Figure 15 and show a strong linear trend with buckling or wrinkling. It is useful to compare the results between the differing geometries of this element set up and that used for the smaller cylinders. The shear strain is directly related to the ratio of radius to length of the cylinder. In the larger tests the ratio, and the resulting shear strain, is almost 2.5 times that of the smaller articles. The shear stress is related to the polar moment of inertia and the radius. The much larger radius increases the polar moment of inertia by close to 60 times. This in turn dominates the effect of the increase in radius on the shear stress and reduces the stress felt by the article. The maximum stress is reduced by 35 times. Because the stresses felt are so low, the element test data is useful mainly for analyses verification and not shear stiffness determination.

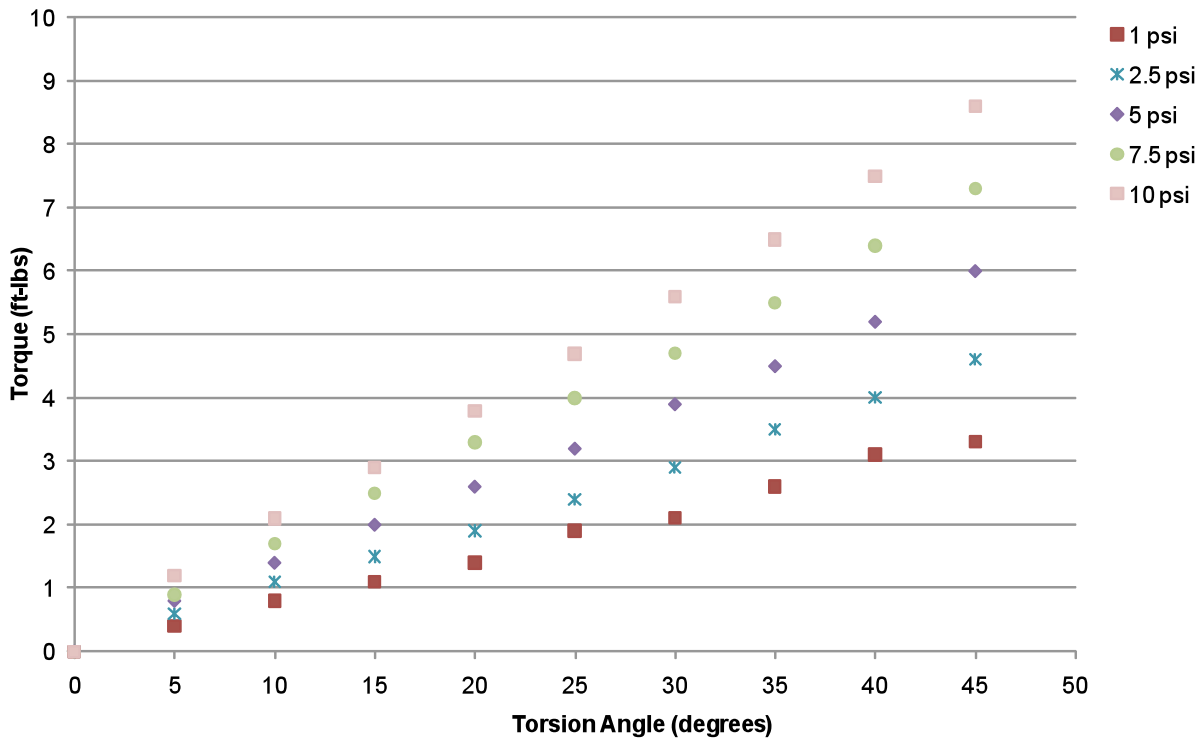


Figure 14. IRVE material cylinder torsion results for increasing inflation pressures. Like the dual-wall IRVE material element, the relationship between torsion and angle of rotation is linear. No wrinkling or buckling was seen in the test.

The Kapton coated Kevlar had a much higher initial torque required to apply an angular deformation, but buckled and lost load carrying ability early in the testing. The results are shown in Figure 15. It should be noted that the results for the smaller cylinders of this Kapton coated Kevlar material did not exhibit the same buckling behavior. Because the cylinder was at a high internal pressure and had a much smaller radius its inherent stiffness was much higher than that exhibited by the larger samples. To reach the same region of stress-strain behavior with the larger element the internal pressure must be increased.

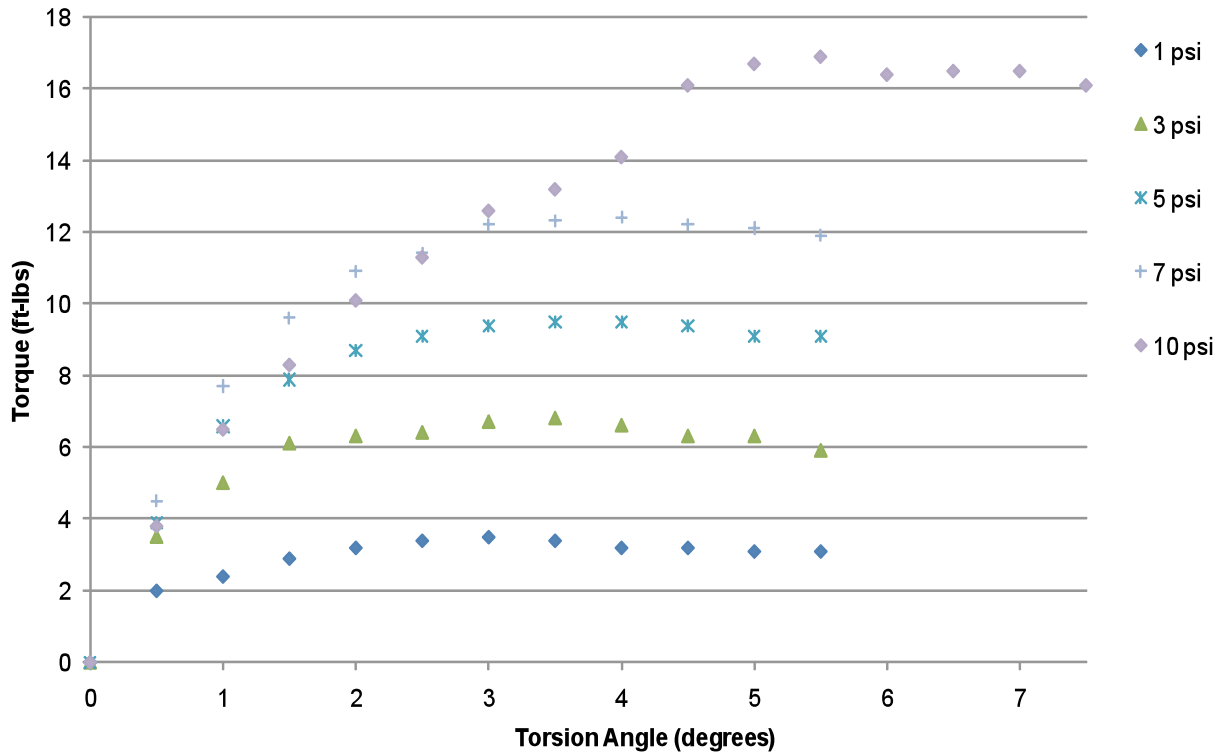


Figure 15. ILC material cylinder torsion results for increasing inflation pressures. This element also shows a leveling of torque required as buckling occurs.

Comparing the results at different pressures between the two elements shows the higher stiffness of the ILC material. Figure 16 includes results from 5 degrees and 10 degrees of rotation for the dual wall elements where the upper two curves are the new ILC material made out of Kapton coated Kevlar and the lower two are the silicone coated Kevlar material used on IRVE. The cylinders exhibited a similar trend, shown in Figure 17 for 5 degrees.

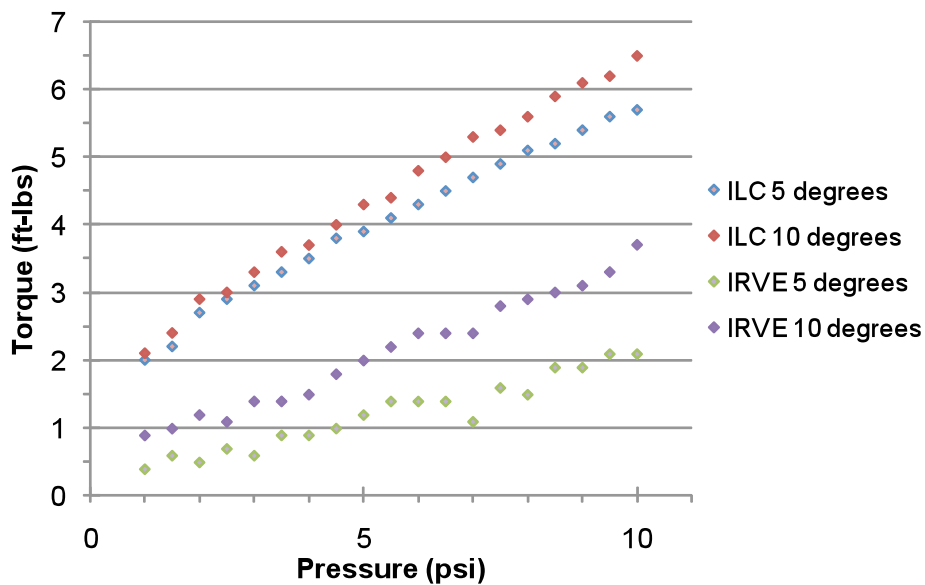


Figure 16. A comparison between the ILC and IRVE materials shows an increase in stiffness at the lower torsion angles. Above a certain angle the dual wall of ILC material buckles.

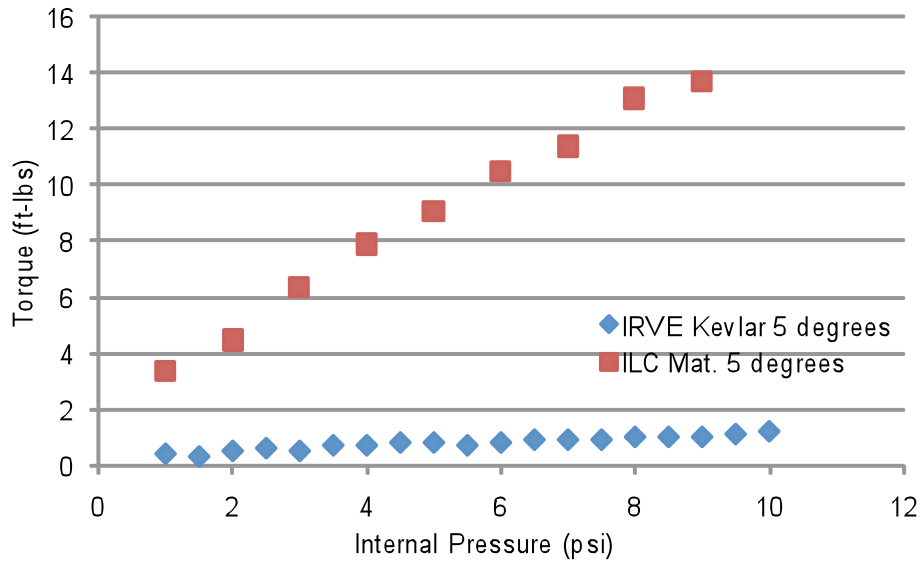


Figure 17. A comparison between the ILC and IRVE materials in the cylinder test also shows an increase in stiffness at the lower torsion angle of 5 degrees. Above a certain angle the cylinder of ILC material wrinkles and then buckles.

VIII. Comparison with Finite Element Analysis

To investigate the validity of the preceding results some initial finite element analysis was completed in LS-DYNA for the simple disk case. The mesh used for all cases run had 2656 elements and 2745 nodes, and is shown in Figure 18. A linear orthotropic model was assumed and each candidate material used is listed in Table 8 where the fill and warp moduli were the apparent modulus from the disk testing, the Poisson’s ratio was assumed to be low, and the shear modulus is varied with internal pressure as calculated. The results for the ILC material are shown in Figure 18. For lower pressures the analytical results match the experiment. As the pressure increases the stiffness is over estimated by the model, which is a phenomena experienced in previous analyses [15].

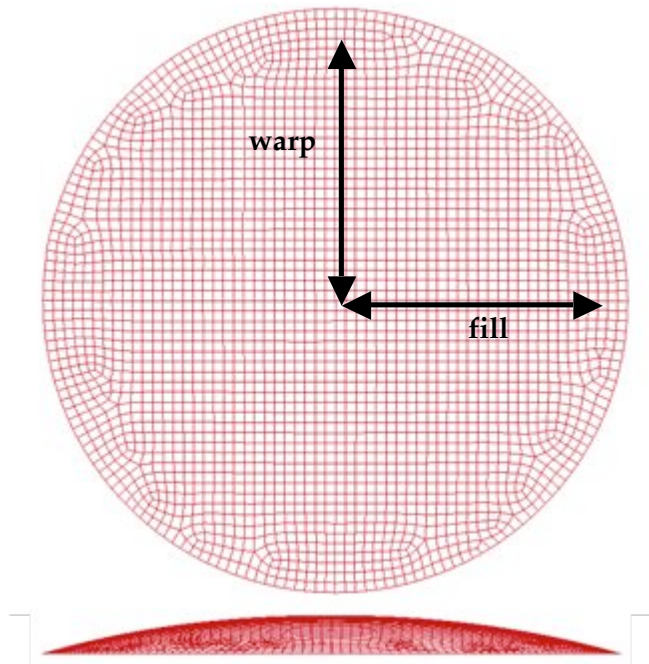


Figure 18. The mesh used for the stress and deflection analysis along with an example deflection result.

Table 8. Kapton coated Kevlar material properties used in the disk model.

Properties	Value
E_1	2.13E+06
E_2	1.78E+06
G	2.54E+04

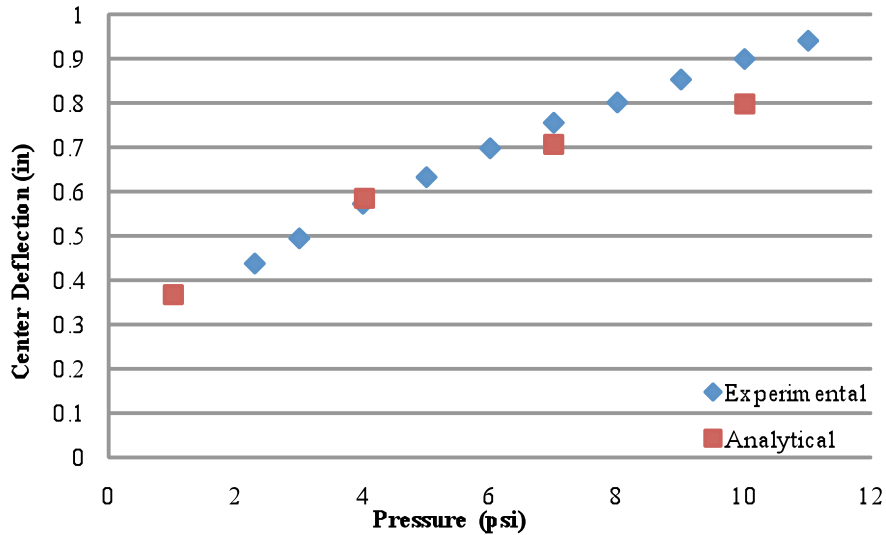


Figure 19. Comparison of the center point deflection for the ILC material between experimental data and analytical results.

IX. Evaluation of Methodologies and Recommendations

The shear behavior of the different candidate materials exhibited a linear elastic behavior at a specific inflation pressure. Because the shear modulus is dependent on the current pressure, the material model should be adjusted accordingly. The biaxial testing of the disks exhibited varying results. The MER/MPF material and the IRVE material did not behave linearly. The PAIDAE material had linear trends as shown in Figure 28, but the new ILC material showed an even stronger linear behavior.

A number of test recommendations can be made regarding the fidelity of the cylinder test setup:

- (1) The magnitude of the deflection in the shear testing was much greater than that created by applying only inflation to the cylinder. This led to difficulties in tracking the strain by use of the photogrammetry due to the small scale of deformation. In future testing the setup should be qualified to higher pressures to allow a larger amount of strain to occur. This would incur higher necessary safety precautions, but improve the calculated results.
- (2) The cylindrical test set up should be designed with a mechanism to apply an axial load in order to control the stress state in the cylinder. This would allow more than just the two to one stress ratio induced by inflation. ILC Dover has incorporated these recommendations and developed a cylindrical test apparatus that will be available for future IAD material testing work. Some specifications for this system include a 30-psig maximum pressure, an 18-inch cylinder diameter, and an axial load of over 7000 pounds. This new test set up will allow these properties to be solved for directly. Using a cylinder compression and torsion test to characterize the material is appropriate than the normal planar biaxial tests because the loading is more representative to actual use of the fabric.
- (3) Though photogrammetry provided a non-invasive method for obtaining strain measurements it was a time intensive technique. The determination of mechanical properties would be made more feasible by including precise sensors for measurement of cylinder rotation, elongation, and if possible inflation.

X. Future Work

Two different areas of research could provide a large amount of benefit to the characterization of woven fabric material properties. The first is an investigation into the current state of mathematical modeling of the mechanics of woven fabrics. There has been a large amount of study already done on this topic and many models exist. They are dependent on variables such as individual fiber thickness, the bend angles, and fibers strengths, but determination of accuracy is necessary. It remains to be determined if this method could be applied without too much investment but it is worth exploring.

The second area of work is a complete trade of material property sensitivity. Simple finite element analyses of the cylinder and disk tests could be run for a wide range of the inputs in order to determine how much the resulting stress and deflection actually vary. This will answer the question of how accurate the determination of mechanical properties actually needs to be and will affect how precise future test apparatus must be built.

XI. Concluding Remarks

A materials test program was conducted to determine the material inputs for finite element models of coated woven fabric inflatable aerodynamic decelerators. Data was collected using tension testing to determine the uniaxial Young's modulus. Biaxial testing was conducted with both a cylinder inflation/torsion test and an inflated disk test to determine the orthotropic mechanical properties. A comparison between the accuracy of using linear elastic Hooke's Law constitutive models for the observed behavior was begun. The results for the shear stress calculations show agreement with predicted linear elastic behavior. The biaxial measurements made in this effort show varying degrees of linearity depending on the test material. Load versus deflection data has been gathered for materials and design techniques planned for upcoming IAD design efforts.

Acknowledgments

This study is a subset of an ILC Dover project, "Advanced Flexible Materials and Systems for Hypersonic and Supersonic Deployable Aeroshells and Decelerators" funded by NASA Langley Research Center. The purpose of the project is to mature inflatable technologies required for High Mass Mars Entry Systems that may enable the exploration of Mars and other planets. I thank the engineers at ILC Dover, especially Joe Welch and Joanne Ware, for their advice and support in planning and conducting these tests, and for creating all the necessary specimens. I also thank the numerous students and staff at Georgia Institute of Technology who helped in conducting and facilitating the tests.

References

- ¹R.D. Braun and R.M. Manning, "Mars Exploration Entry, Descent, and Landing Challenges," *Journal of Spacecraft and Rockets*, vol. 44, no. 2, pp. 310-323, March-April 2007.
- ²I.G. Clark, A.L. Hutchings, C.L. Tanner, R.D. Braun. "Supersonic Inflatable Aerodynamic Decelerators for Use on Future Robotic Missions to Mars." *Journal of Spacecraft and Rockets*. Vol. 46, No. 2. March-April 2009.
- ³R.R. Barton, "Development of Attached Inflatable Decelerators for Supersonic Application." NASA CR-66613, 1968.
- ⁴D.A. Shockey, D.C. Erlich, and J.W. Simons, 1999, "Lightweight Fragment Barriers for Commercial Aircraft." *18th International Symposium on Ballistics*, pp. 1192-1199.
- ⁵"Abaqus Analysis User's Manual Version 6.8", Providence RI, Dassault Systemes Simulia Corp., 2008
- ⁶R.J. Bassett, R. Postle, N. Pan. "Experimental Methods for Measuring Fabric Mechanical Properties: A Review and Analysis." *Textile Research Journal*. Vol. 69. 1999. P. 866-875.
- ⁷H.W. Reinhardt. "On the Biaxial Testing and Strength of Coated Fabrics." *Experimental Mechanics*. Vol. 16, No. 2. February 1976. P. 71-74.
- ⁸ASTM D5035-06. "Standard Test Method for Breaking Force and Elongation of Textile Fabrics (Strip Method)."
- ⁹P.V. Cavallaro, A.M. Sadegh, C.J. Quigley. "Contributions of Strain Energy and *PV-work* on the Bending Behavior of Uncoated Plain-woven Fabric Air Beams." *Journal of Engineering Fibers and Fabrics*. Vol. 2, No. 1. 2007. P. 16-30.
- ¹⁰A. Makris, C. Ramault, A. Smits, D. Van Hemelrijck, A. Clarke, C. Williamson, M. Gower, R. Shaw, R. Mera, E. Lamkanfi, W. Van Paepegem. "A review of biaxial test methods for composites." *Experimental Analysis of Nano and Engineering Materials and Structures*. Springer Netherlands. 2007.

¹¹M. Said. "Biaxial Test Method for Characterization of Fabric-Film Laminates Used in Scientific Balloons." *Journal of Industrial Textiles*. Vol. 30, No. 4. April 2001. P. 280-288.

¹²A.W. Turner, J.P. Kabche, M.L. Peterson, W.G. Davids. "Tension/Torsion Testing of Inflatable Fabric Tubes." *Experimental Techniques*. Vol. 32, No. 2. March/April 2008. P. 47-52.

¹³R.S. Pappa, L.R. Giersch, J.M. Quagliaroli. "Photogrammetry of a 5m inflatable space antenna with consumer grade digital cameras." *Experimental Techniques*. July/August 2001. P. 21- 29.

¹⁴J. Welch , S.Wang, J. Blandino, K. McEvoy. "Super Pressure Balloon Non-Linear Structural Analysis and Correlation Using Photogrammetric Measurements." *AIAA 5th ATIO and 16th Lighter-Than-Air Sys Tech. and Balloon Systems Conferences*, Arlington, Virginia, Sep. 26-28, 2005. AIAA-2005-7447

¹⁵J.R. Rowe, S.W. Smith, A. Simpson, J. Jacob "Development of a Finite Element Model of Warping Inflatable Wings." *47th AIAA/ASME/AHS/ASC Structures, Structural Dynamics, and Materials Conference*, Newport, Rhode Island, May 1-4, 2006. AIAA-2006-1697

Appendix A: Uniaxial Testing Results

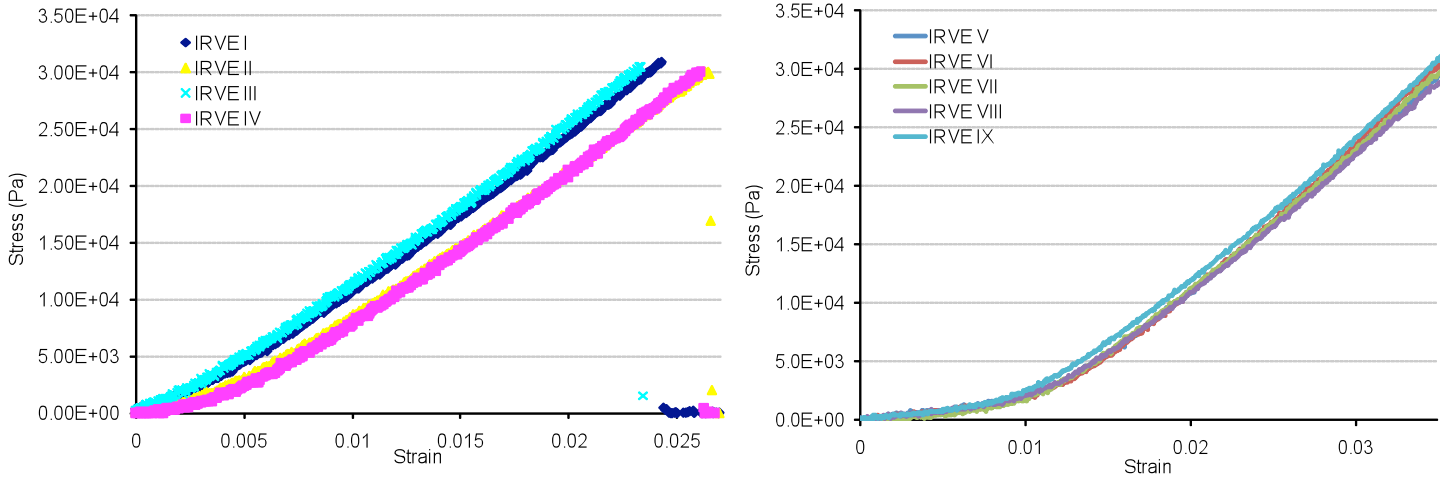


Figure 20. Uniaxial stress-strain curve for the double sided silicone coated Kevlar used on the IRVE project in the warp direction (left) and the fill direction (right).

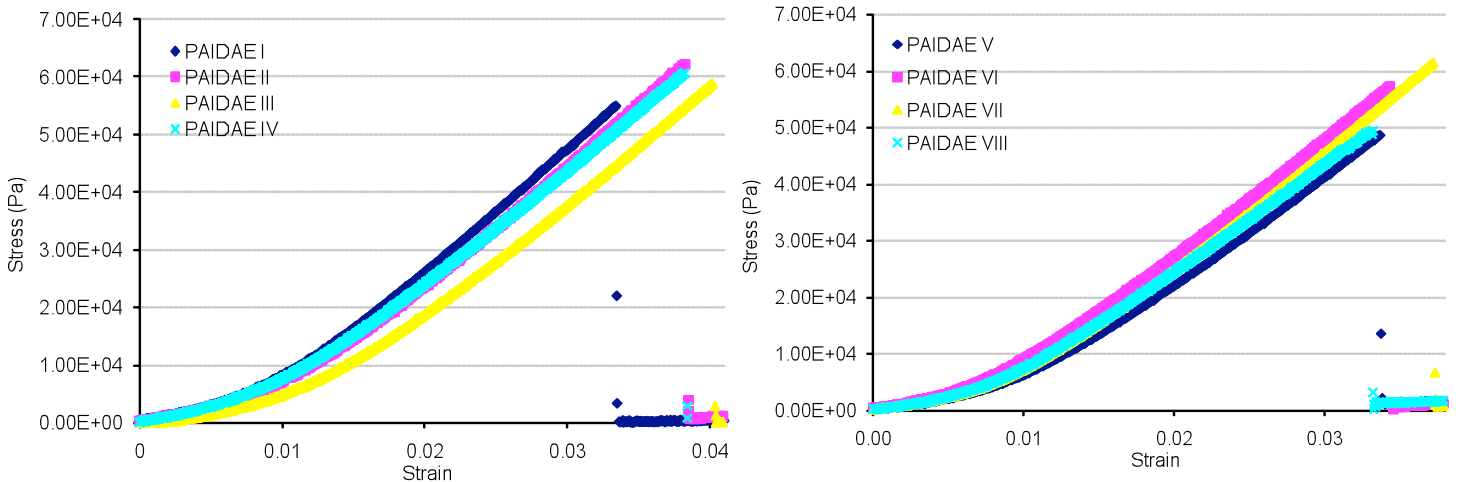


Figure 21. Uniaxial stress-strain curve for the single sided silicone coated Kevlar used on the PAIDAE wind tunnel tests of a tension cone in the warp direction (left) and fill direction (right).

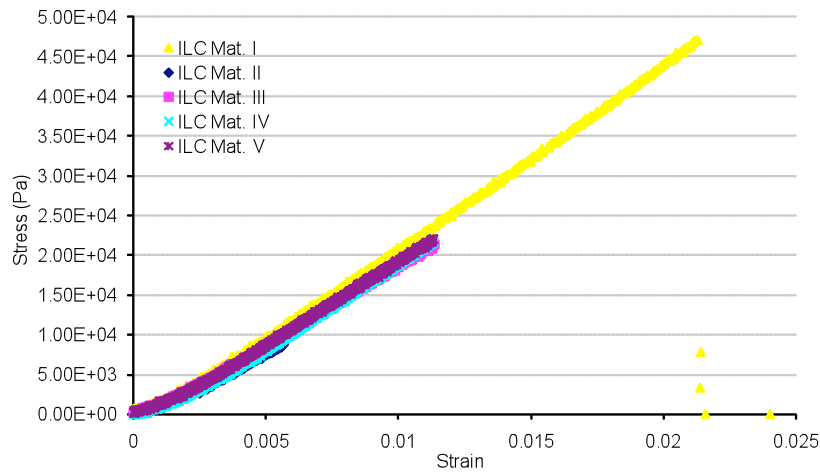


Figure 22. Uniaxial stress-strain curve for the Kapton coated Kevlar in the warp direction. All samples beyond the first were tested to approximately 50 percent of the breaking strength to avoid jaw break.

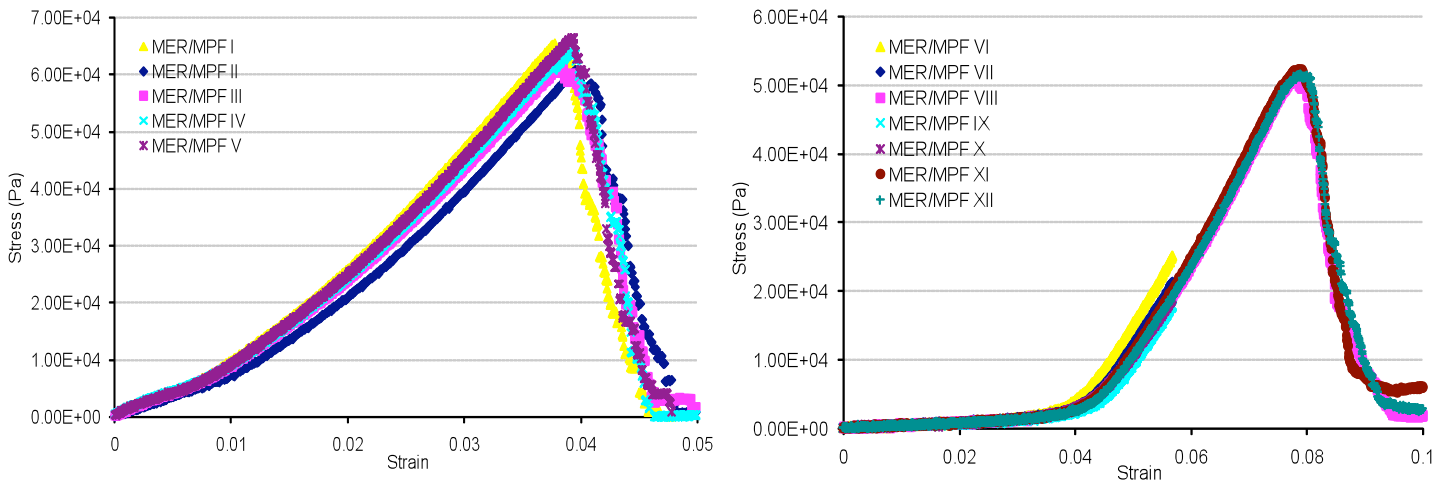


Figure 23. Uniaxial stress-strain curve for the Vectran in the warp (left) and fill (right) directions.

Appendix B: Cylinder Shear Results

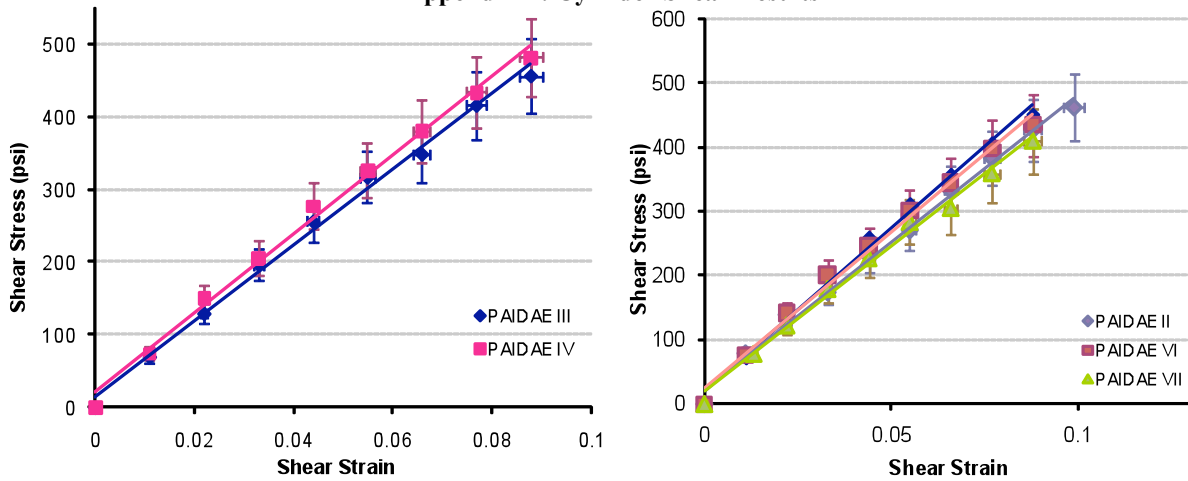


Figure 24. Shear results for the double sided silicone coated Kevlar material in the warp (left) and fill (right) directions.

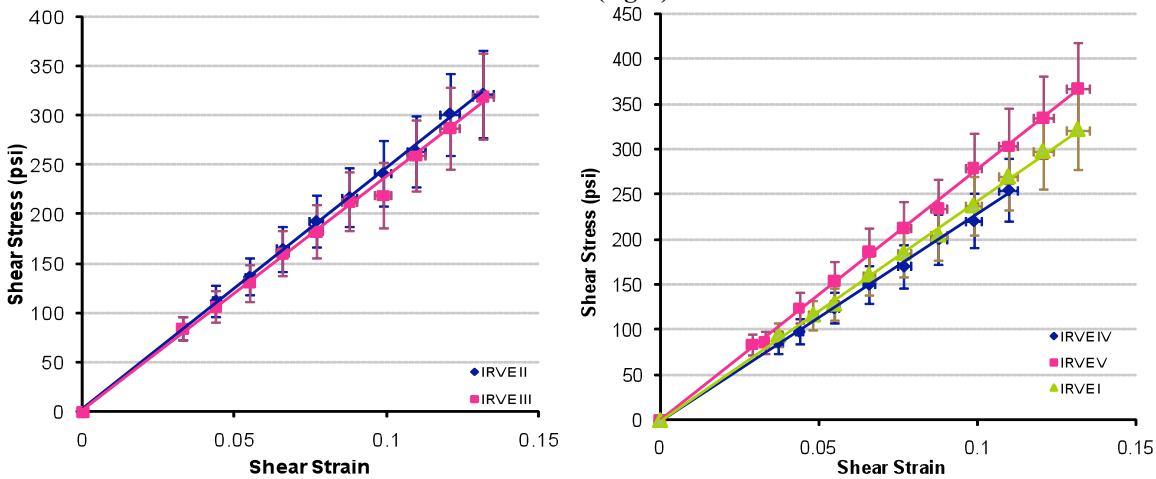


Figure 25. Shear results for the single sided silicone coated Kevlar material in the warp (left) and fill (right) directions.

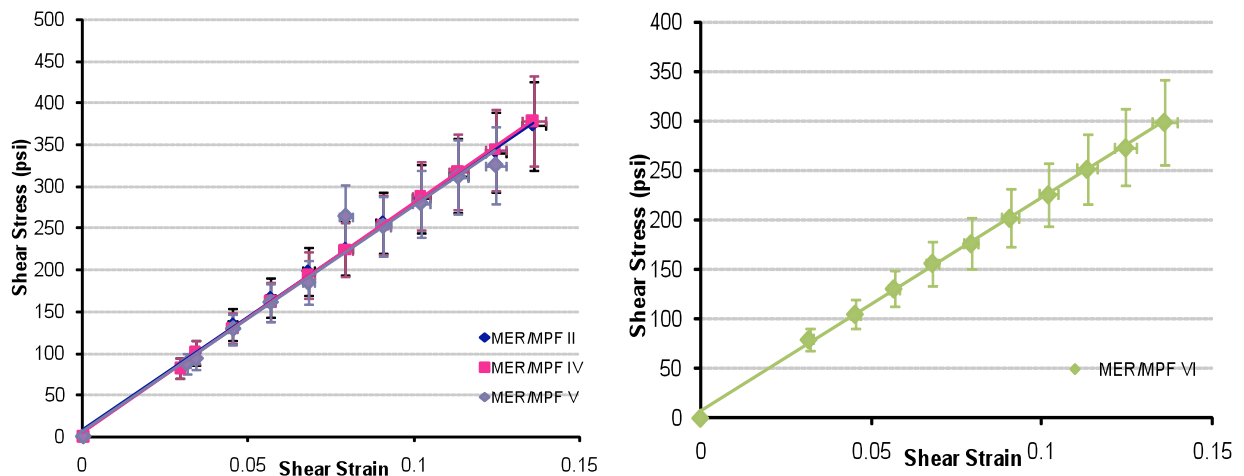


Figure 26. Shear results for the Vectran material used in the warp (left) and fill (right) directions

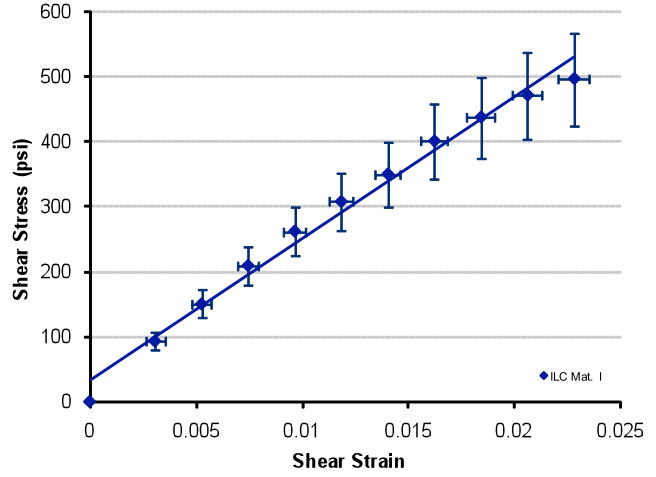
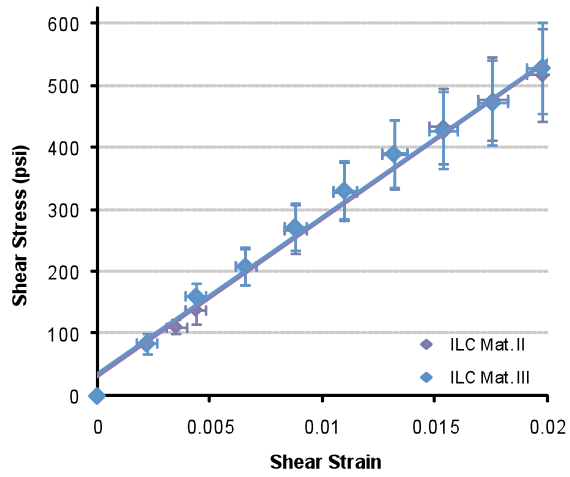


Figure 27. Shear results for the Kapton coated Kevlar material in the warp (left) and the fill (right) directions.

Appendix C: Disk Test Results

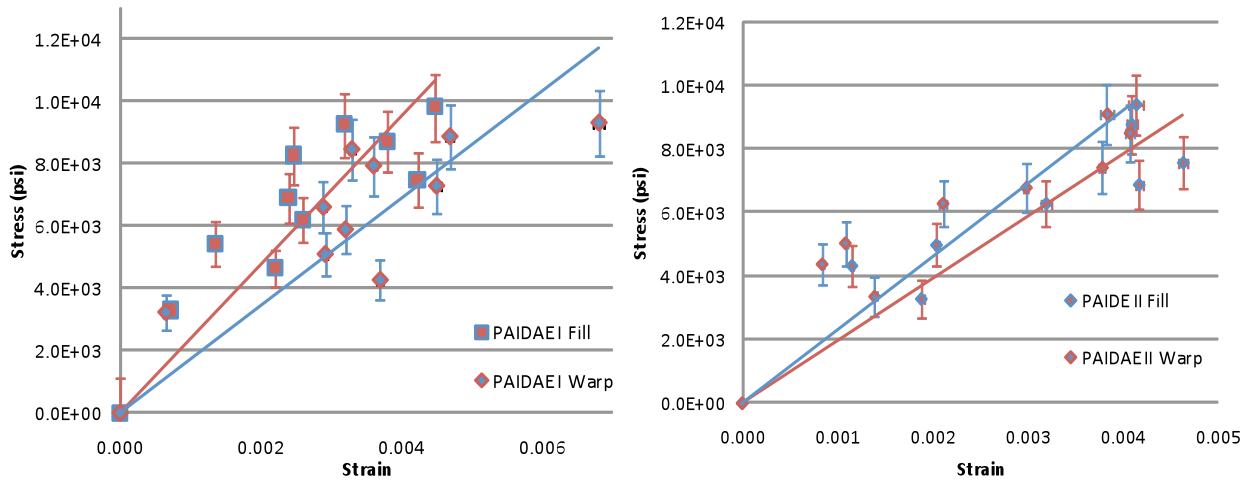


Figure 28. Stress in the two principal directions for the double sided silicone coated Kevlar material for two runs.

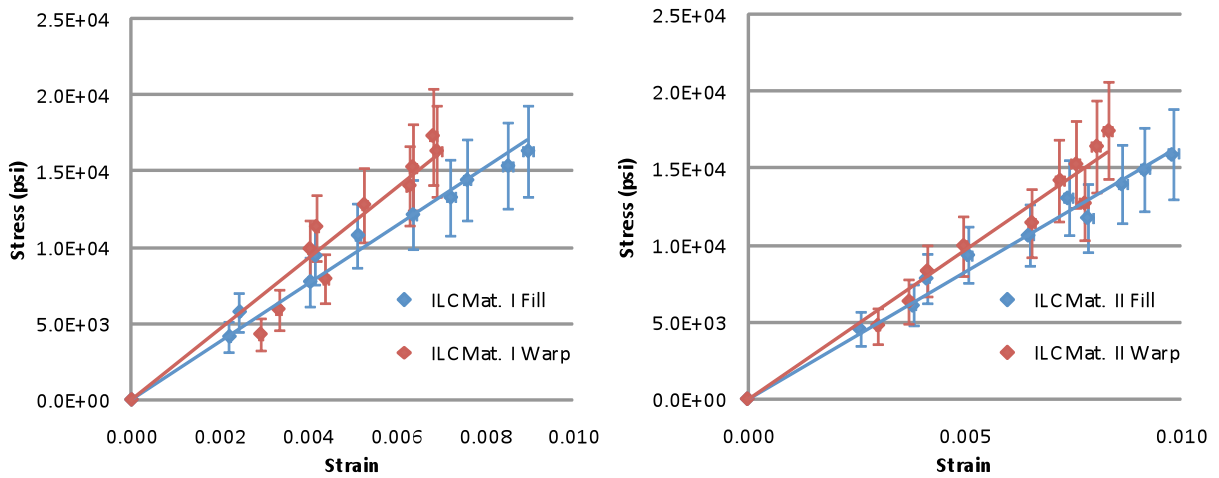


Figure 29. Stress in the two principal directions for the Kapton coated Kevlar material for two runs.